

# Waveguide-coupled single NV in diamond enabled by femtosecond laser writing

J. P. HADDEN<sup>1,†,\*</sup>, V. BHARADWAJ<sup>2,†</sup>, B. SOTILLO<sup>3</sup>, S. RAMPINI<sup>3</sup>, R. OSELLAME<sup>3</sup>, J. WITMER<sup>1,5</sup>, H. JAYAKUMAR<sup>1,6</sup>, T. T. FERNANDEZ<sup>2,3</sup>, A. CHIAPPINI<sup>4</sup>, C. ARMELLINI<sup>4</sup>, M. FERRARI<sup>4</sup>, R. RAMPONI<sup>2,3</sup>, P. E. BARCLAY<sup>1</sup>, S. M. EATON<sup>2,3</sup>

<sup>1</sup>*Institute for Quantum Science and Technology, University of Calgary, Calgary*

<sup>2</sup>*Department of Physics, Politecnico di Milano, Piazza Leonardo da Vinci 32, Milano, Italy*

<sup>3</sup>*Istituto di Fotonica e Nanotecnologie-Consiglio Nazionale delle Ricerche (IFN-CNR), Piazza Leonardo da Vinci 32, Milano, Italy*

<sup>4</sup>*Istituto di Fotonica e Nanotecnologie (IFN)-CNR, CSMFO and FBK-CMM, Trento, Italy*

<sup>5</sup>*Department of Physics, City University of New York (CUNY)–City College of New York, New York, NY 10031, USA*

<sup>6</sup>*Ginzton Laboratory, Stanford University, Stanford, CA 94305, USA*

\*Corresponding author: [jpe.hadden@gmail.com](mailto:jpe.hadden@gmail.com)

**Diamond's nitrogen vacancy (NV) center is an optically active defect with long spin coherence time, showing excellent promise for efficient nanoscale magnetic field sensing and long-range entanglement schemes. Recently, femtosecond laser writing demonstrated the formation of buried 3D optical waveguides and high quality single NV centers in diamond. However, combining these technologies was an outstanding challenge. In this work, photonic circuits aligned with submicron resolution to single NVs are fabricated in diamond using femtosecond laser writing, to enable an integrated platform for the excitation and collection from NVs. This fabrication technology opens the way towards optically integrated spin-based magnetic field sensing as well as on-chip optical routing of single photons between NVs.**

OCIS codes: (230.7370) Waveguides; (350.3390) Laser materials processing; (320.2250) Femtosecond phenomena; (220.1920) Diamond machining; (270.5585) Quantum information and processing; (270.0270) Quantum optics

Diamond's nitrogen-vacancy (NV) color center is a point defect consisting of a nearest-neighbor pair of a nitrogen atom, which substitutes for a carbon atom, and a lattice vacancy. These optically active negatively charged defects have long room temperature spin coherence time, making them promising for nanoscale magnetic field sensing [1] and for quantum information systems [2]. An integrated photonics platform in diamond would be beneficial for NV-based optically detected spin magnetometry, and quantum computing, in which NV centers are optically linked for long-range quantum entanglement due to the integration and stability provided by monolithic optical waveguides [3].

Recently, the versatile femtosecond laser microfabrication method demonstrated buried 3D optical waveguides in diamond [4, 5], a key first step towards a diamond photonics platform. However, for practical implementation of quantum information systems and magnetometry devices, the deterministic placement of NVs is required.

The most widely used method to place NV centers in diamond relies on ion or electron implantation followed by annealing to form NV centers [6, 7]. This method offers submicron spatial accuracy and significant progress has been made in the development of annealing processes to repair unwanted damage to the lattice which can degrade the NV centers properties, especially for shallow centers [8, 9]. However the increased energy required for deeper NV creation causes even more damage [10] thus techniques which allow the ability to place NV centers in buried structures with minimal damage are preferable.

In 2013, it was shown that NV centers could be produced in optical grade diamond by exploiting the electron plasma created by femtosecond laser pulses focused just above the surface [11]. This technique however was limited to near-surface placement of NVs and caused ablative damage of the diamond surface, which is detrimental for applications. Recently, Chen *et al.* demonstrated significant improvement on this initial result, with on-demand and high quality single NVs written in the bulk of ultrapure quantum grade diamond (nitrogen concentration of <5 ppb) using femtosecond laser microfabrication with a spatial light modulator (SLM) to correct for aberrations [12], combined with high temperature annealing of the diamond sample.

In this Letter, we apply femtosecond laser writing to inscribe optical waveguides within ultrapure diamond, along with a static laser exposure centered within the waveguides for NV creation. Crucially, we find that the optical waveguide properties remain unchanged after annealing the sample to allow vacancies formed within the static exposure to diffuse and combine with a nitrogen impurity to create a single NV. Due to using the same laser and positioning system to form both waveguides and NVs, the NV and optical waveguide mode are aligned within submicron resolution.

We further demonstrate waveguide excitation and collection of light from these laser-formed single NVs. Such waveguide coupled NVs could open the door for more sophisticated quantum photonic networks in diamond. For example, in quantum grade diamond, the optically linked single NVs could be exploited for single photon sources or solid state qubits [13-15]. In lower purity diamond, the laser writing of high density NV ensembles within waveguides could enable robust

excitation and collection of the fluorescence signal for magnetometry [16, 17].

The femtosecond laser used for waveguide writing in diamond was a regeneratively amplified Yb:KGW system (Pharos, Light Conversion) with 230 fs pulse duration, 515 nm wavelength and 500 kHz repetition. The femtosecond laser pulses were focused below the diamond surface with a 1.25 NA oil immersion lens (RMS100X-O 100× Plan Achromat Oil Immersion Objective, Olympus). Computer-controlled 3-axis motion stages (ABL1000, Aerotech) were used to translate the quantum grade diamond sample (2 mm × 2 mm × 0.3 mm, nitrogen impurities <5 ppb, MB optics) transversely relative to the laser to form the optical waveguides.

Figure 1 shows an overhead schematic (a) and optical microscope image (b) of the waveguide-NV optical device in diamond. In order to calibrate the depth and pulse energy of the NV creation relative to the waveguide formation, multiple test waveguides with an NV center in them were written. In this paper, we focus on one waveguide with NV centers created at the corresponding depth.

The optical waveguide was formed at 25  $\mu\text{m}$  depth (measured from surface to center of modifications) with processing conditions of 500 kHz repetition rate, 60 nJ pulse energy, 0.5 mm/s scan speed, and 13  $\mu\text{m}$  separation between modification lines. Because focused femtosecond laser pulses yield an amorphization in crystalline diamond, the type II geometry [18] was adopted, where two closely spaced modification lines provide optical confinement. A higher pulse energy of 100 nJ was required in our previous study [4] because of the larger depth (40  $\mu\text{m}$ ), resulting in increased spherical aberration and therefore distortion in the intensity distribution at the focus.

Despite the shallower writing depth and higher purity of diamond used in the present study, the waveguides were found to have similar guiding properties as in our previous work [4], with a symmetric mode with a mode field diameter of 10  $\mu\text{m}$  at 635 nm wavelength (Fig. 1(c)). The near field mode profile was measured by imaging the output facet with a 60× asphere to a CCD (SP620U, Spiricon). The insertion loss was 5 dB at 635 nm wavelength (TLS001-635, Thorlabs) for the TM polarization launched with a PM fiber.

One improvement compared to our previous result is that the present waveguide revealed only a single guiding location. We attribute this transition to single mode guiding to the reduced spherical aberration at shallower depths, which results in less vertical elongation of the laser-induced modifications and therefore a more confined guiding region [19].

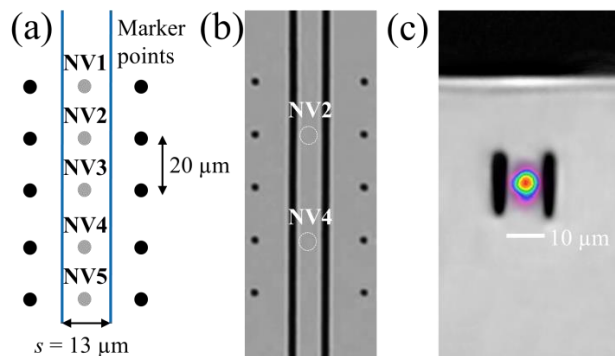


Fig. 1. (a) Overhead schematic of waveguide-NV device in diamond, showing five static single-pulse (24 nJ pulse energy) femtosecond laser exposures separated axially by 20  $\mu\text{m}$ . The depth of the single-pulse exposures was 25  $\mu\text{m}$ , and centered within the cross section of the laser-fabricated waveguide. Marker points were written (100 nJ pulse energy, 25 pulses) outside of the waveguide to locate the axial position

of the single pulse exposures, which are not visible by optical microscopy. (c) Transverse view optical microscope image of type II waveguide in diamond and overlaid mode profile at 635 nm wavelength.

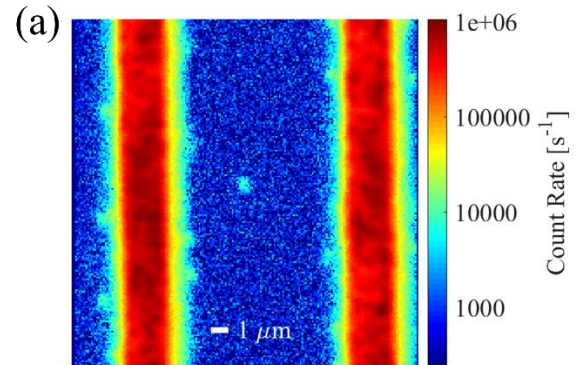


Fig. 2. Overhead confocal photoluminescence intensity map showing NV2 within optical waveguide when excited from above using a 0.8 NA objective.

Using the same femtosecond laser setup, single-pulse femtosecond static exposures were inscribed within the optical waveguide to induce vacancies in the diamond lattice. The pulse energy for the static exposures was 24 nJ, below the single pulse damage threshold (~50 nJ) in diamond. Five identical static exposures separated by 20  $\mu\text{m}$  were written in order to study the reproducibility in forming single NV centers within the waveguiding region. The depth of the static exposures was 25  $\mu\text{m}$ , and centered within the cross section of the laser-fabricated waveguide. Marker points were inscribed (100 nJ pulse energy, 25 pulses) outside of the waveguide to axially locate the single pulse exposures, which are not visible by optical microscopy.

The quantum grade diamond sample was subsequently annealed in order to form NV centers. Vacancies, which become mobile above 600°C, are captured by substitutional nitrogen [7]. In a sample of this type there can be 100-1000 nitrogen impurities present within the  $\sim(1 \mu\text{m})^3$  focal volume of the focused femtosecond laser beam. It has been shown that annealing at higher temperatures (1000°C and above) improved the characteristics of the NV centers, as other vacancy complexes which can be detrimental are annealed out [8, 9]. The annealing was performed in a tubular horizontal furnace (LTF15/50/450, Lenton) at 1000°C for 3 hours in a nitrogen atmosphere, to avoid oxidation at the diamond surface.

At that temperature, the bulk material does not suffer structural changes or graphitization [20]. Previous studies in other crystals have shown that high temperature annealing can erase the waveguides produced by femtosecond laser irradiation [21, 22], mainly due to the disappearance of the stressed guiding region or the recovery of the crystalline structure. In the case of diamond, the laser modification tracks remain after annealing, as the diamond crystal lattice cannot be restored with this process [23]. From  $\mu\text{Raman}$  measurements done on the laser-written lines, we observed the formation of a higher concentration of graphite nanoclusters inside the amorphous carbon matrix after annealing, consistent with other studies [23, 24]. However, to quantify this increase in graphite, TEM analysis is necessary.

Even with the increased graphite inside the modification lines, the diamond guiding region is unchanged, where we observed a similar diamond Raman peak width (i.e. crystal quality) and shift (i.e. stress distribution) after annealing. This indicates that the crystalline structure is not altered and the stress is not relieved, as the damage lines are still present [25]. Crucially we found that the mode profile and

insertion loss of the annealed waveguides were unaltered, which indicates the temperature required to cause waveguide degradation is higher than that required to form the NVs.

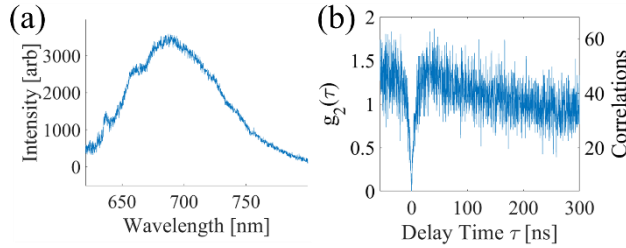


Fig. 3. Properties of single NV written with 24 nJ energy static femtosecond laser exposure followed by annealing. (a) PL spectrum showing signature ZPL at 637 nm and phonon side band, (b) Intensity autocorrelation revealing single photon emission.

Unlike Chen *et al.* [12], we did not use a spatial light modulator to compensate for spherical aberration to produce optical waveguides and NV centers. We found that single NVs could be formed in quantum grade diamond at depths shallower than 30  $\mu\text{m}$ . As shown by the circled regions in the overhead microscope image of the waveguide - NV circuit in Fig. 1(b), two of the five static exposures, NV2 and NV4, showed single NVs after annealing, as described below. This 40% probability of creating single NVs is consistent with the results of SLM-aided laser writing of NV centers [12].

Initial overhead photoluminescence (PL) characterization was performed using a homebuilt confocal microscope. A DPSS 532 nm laser (CL532-500-L, CrystaLaser) was focused onto the sample through a 0.8 NA objective (100 $\times$  CFI60 TU Plan Epi ELWD, Nikon) mounted on a closed loop piezo positioning stage (Tritor 101, PiezosystemJena). The induced PL was collected through the same objective, filtered from the excitation, and Raman scattered light using a dichroic beam splitter (ZT 532 RDC, Chroma) and long-pass filters (555 nm long pass, ET 555 LP Chroma, 650 nm long pass, FELH 0650 Thorlabs) to allow only the NV broadband phonon sideband to pass. This light was focused into a single mode fiber which provided the confocal aperture. Photon counting of the filtered light was performed using an avalanche photodiode (SPQR-14, Perkin-Elmer). An overhead PL confocal raster scan of the region where the NV2 trial was written shows a bright spot corresponding to NV2 between the two bright laser modified lines (Fig. 2)

For both NV2 and NV4, we estimate they are  $\sim 1 \mu\text{m}$  shallower than the center of laser-modified lines and hence the peak of the optical mode. We selected NV2 for waveguide coupling experiments as its lateral position (shifted in  $x$  by  $+0.7 \mu\text{m}$ , shown in Fig. 2) is better centered compared to NV4 (shifted in  $x$  by  $+0.9 \mu\text{m}$ ). The  $\sim 1 \mu\text{m}$  shift of the NV2 and NV4 is larger than the maximum shifts of  $\sim 600 \text{ nm}$  reported previously [12], which we attribute to the larger focal volume provided by our beam delivery setup. All measurements reported below refer to NV2.

Figure 3(a) shows the PL spectrum recorded at room temperature from the NV with the 650 nm long pass filter removed, where the characteristic ZPL at 637 nm and the broadband phonon side band are clearly visible. An intensity autocorrelation measurement  $g^{(2)}(\tau)$  of this emission is shown in Fig. 3(b), showing the antibunching dip with  $g^{(2)}(0)$  well below 0.5, characteristic of single photon source emission.

In order to demonstrate the ability to guide 532 nm excitation light through the waveguide to the NV center, the output from the excitation laser was coupled to the laser-written waveguide by butt-coupling a single mode fiber (460HP, Thorlabs) to the input facet of the diamond

waveguide. Index matching oil (Type A,  $n_e = 1.518$ , Cargille) was used to improve the transmission and coupling stability. A fraction of the high intensity light within the waveguide undergoes Raman scattering, with the first order Raman shift at 572 nm. Some of this scattered light is emitted out of the waveguide, and can be detected through the confocal microscope's collection arm with the 650 nm long pass filter removed. Figure 4(a) shows a confocal collection raster scan of a larger area of the sample, revealing the Raman scattering due to the waveguided light. The waveguide alignment was optimized by observing the near field intensity from the output facet of the waveguide using a 0.42 NA objective (50 $\times$  Plan Apo SL Infinity Corrected, Mitutoyo) coupled to a CCD.

The waveguide coupled excitation of the NV center is demonstrated in Fig. 4(b) and (c), with collection of the NV center's emitted light through the overhead confocal microscope. A confocal collection raster scan of a small area around NV2 with excitation through the waveguide shows fluorescence from the expected NV position (Fig. 4(b)). Verification is achieved by the use of a back-illuminated EMCCD (DU-897U-CS0-#BV iXon Ultra, Andor) with 12 $\times$  zoom lens (UltraZoom non-FF, Navitar), which again shows emission located to the NV position (Fig. 4(c)).

The relatively modest detected photon count rate of 10 counts/s, above the background in Fig. 4(a) is expected given that the mode size of the waveguide ( $\sim 10 \mu\text{m}$ ) is much larger than the focused spot from free space excitation 0.8 NA lens, ( $\sim 1 \mu\text{m}$ ) resulting in a several orders of magnitude lower power density at the NV center. Indeed identical count rates to the confocal microscope collection rate would be expected for comparable power densities. An increase in the effective power density could be achieved by tailoring the refractive index profile of the written waveguide to achieve a smaller mode field diameter, or by using a more powerful laser.

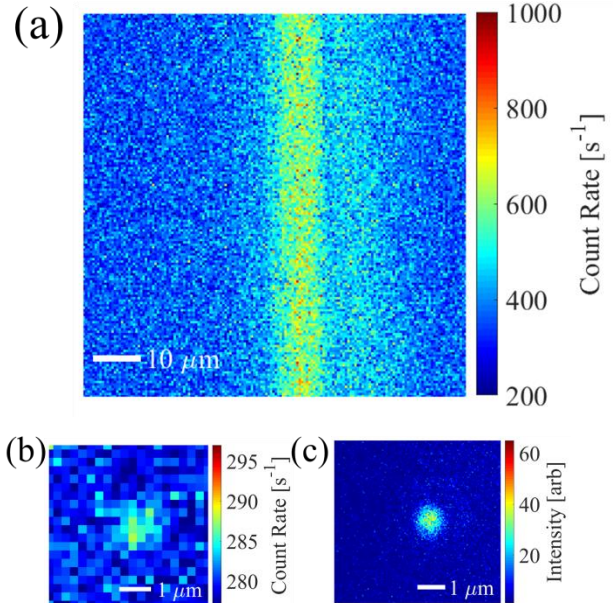


Fig. 4. Overhead views while the 532 nm excitation laser is coupled to the input waveguide facet. (a) Confocal collection raster scan of Raman scattered light. (b) Confocal photoluminescence collection raster scan of single NV and (c) EMCCD image of single NV.

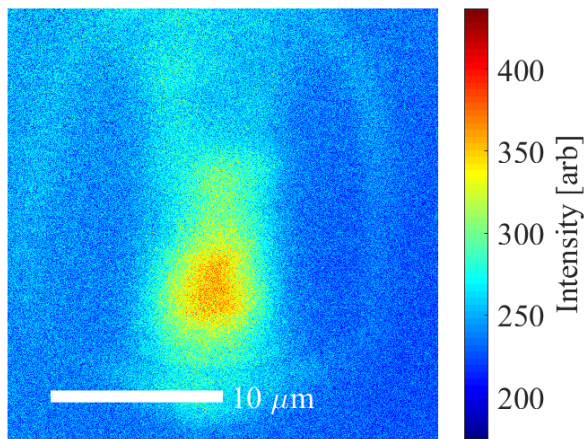


Fig. 5. EMCCD image of the intensity distribution of the NV emission collected by optical waveguide when exciting the NV from the top using a 532 nm laser and 0.8 NA objective. The signal is filtered using a 650 nm long pass filter, and corrected for any remaining Raman or laser by subtracting the recorded signal when exciting the waveguide near the NV center.

Further evidence of waveguide-NV coupling is shown in Fig. 5. In this case, the NV center is excited from overhead through the confocal microscope's objective, while emission is collected through the optical waveguide. The waveguide output facet is imaged onto the EMCCD through a 0.42 NA objective. The intensity distribution of the NV emission (spectral content 650 nm – 800 nm) at the waveguide output (Fig. 5) shows a similar size and shape as the near-field mode profile when coupling the waveguide with a 635 nm wavelength laser diode (Fig. 1(c)).

In summary, we have demonstrated an integrated quantum photonic chip in diamond, fabricated entirely with femtosecond laser writing. The scanned optical waveguides and static exposures to produce vacancies were fabricated in a single processing step, with excellent alignment thanks to the submicron sized focal volume and high resolution computer-controlled positioning stages. The annealing required to unite laser-formed vacancies with nitrogen impurities had no adverse effect on the transmission properties of optical waveguides.

Importantly, we showed that optical waveguides could be used to excite and collect light from single NVs. Further improvement in NV excitation efficiency is expected by reducing the mode size by tailoring of the refractive index profile through optimization of the geometry of the type II waveguide. Optical waveguides coupled to NV centers with arbitrary 3D configurations and integrated in quantum grade diamond could open the door for exciting new possibilities in quantum information processing. Future work will study the formation of NV ensembles in lower grade [17] and delta-doped diamond [26, 27] which will boost the waveguided fluorescence signal for more efficient sensing of magnetic fields.

## FUNDING SOURCES AND ACKNOWLEDGMENTS

**Funding.** FP7 DiamondFab CONCERT Japan project, DIAMANTE MIUR-SIR grant, and FemtoDiamante Cariplo ERC reinforcement grant.

**Acknowledgment.** We thank Prof. Guglielmo Lanzani and Dr. Luigino Criante for the use of the FemtoFab facility at CNST – IIT Milano for the laser fabrication experiments.

## REFERENCES

1. J. M. Taylor, P. Cappellaro, L. Childress, L. Jiang, D. Budker, P. R. Hemmer, A. Yacoby, R. Walsworth, and M. D. Lukin, *Nature Physics* **4**, 810–816 (2008).
2. B. Hensen, H. Bernien, A. E. Drau, A. Reiserer, N. Kalb, M. S. Blok, J. Ruitenberg, R. F. L. Vermeulen, R. N. Schouten, C. Abelln, W. Amaya, V. Pruneri, M. W. Mitchell, M. Markham, D. J. Twitchen, D. Elkouss, S. Wehner, T. H. Taminiau, and R. Hanson, *Nature* **526**, 682–686 (2015).
3. T. Schröder, S. L. Mouradian, J. Zheng, M. E. Trusheim, M. Walsh, E. H. Chen, L. Li, I. Bayn, and D. Englund, *JOSA B* **33**, B65–B83 (2016).
4. B. Sotillo, V. Bharadwaj, J. P. Hadden, M. Sakakura, A. Chiappini, T. T. Fernandez, S. Longhi, O. Jedrkiewicz, Y. Shimotsuma, L. Criante, R. Osellame, G. Galzerano, M. Ferrari, K. Miura, R. Ramponi, P. E. Barclay, and S. M. Eaton, *Scientific Reports* **6**, 35566 (2016).
5. A. Courvoisier, M. J. Booth, and P. S. Salter, *Appl Phys Lett* **109**, 031109 (2016).
6. J. O. Orwa, C. Santori, K. M. C. Fu, B. Gibson, D. Simpson, I. Aharonovich, A. Stacey, A. Cimmino, P. Balog, M. Markham, D. Twitchen, A. D. Greentree, R. G. Beausoleil, and S. Prawer, *Journal of Applied Physics* **109**, 083530 (2011).
7. J. R. Rabeau, P. Reichart, G. Tamanyan, D. N. Jamieson, S. Prawer, F. Jelezko, T. Gaebel, I. Popa, M. Domhan, and J. Wrachtrup, *Appl Phys Lett* **88**, 023113 (2006).
8. B. Naydenov, F. Reinhard, A. Lammle, V. Richter, R. Kalish, U. F. S. D'Haenens-Johansson, M. Newton, F. Jelezko, and J. Wrachtrup, *Appl Phys Lett* **97**, 242511 (2010).
9. T. Yamamoto, T. Umeda, K. Watanabe, S. Onoda, M. L. Markham, D. J. Twitchen, B. Naydenov, L. P. McGuinness, T. Teraji, S. Koizumi, F. Dolde, H. Fedder, J. Honert, J. Wrachtrup, T. Ohshima, F. Jelezko, and J. Isoya, *Physical Review B* **88**, 075206 (2013).
10. S. Pezzagna, B. Naydenov, F. Jelezko, J. Wrachtrup, and J. Meijer, *New Journal of Physics* **12**, 065017 (2010).
11. Y. Liu, G. Chen, M. Song, X. Ci, B. Wu, E. Wu, and H. Zeng, *Optics Express* **21**, 12843 (2013).
12. Y.-C. Chen, P. S. Salter, S. Knauer, L. Weng, A. C. Frangskou, C. J. Stephen, S. N. Ishmael, P. R. Dolan, S. Johnson, B. L. Green, G. W. Morley, M. E. Newton, J. G. Rarity, M. J. Booth, and J. M. Smith, *Nature Photonics* **11**, 77–80 (2016).
13. H. J. Kimble, *Nature* **453**, 1023–1030 (2008).
14. Q. Shi, B. Sontheimer, N. Nikolay, A. W. Schell, J. Fischer, A. Naber, O. Benson, and M. Wegener, *Scientific Reports* **6**, 31135 (2016).
15. A. Sipahigil, R. E. Evans, D. D. Sukachev, M. J. Burek, J. Borregaard, M. K. Bhaskar, C. T. Nguyen, J. L. Pacheco, H. A. Atikian, C. Meuwly, R. M. Camacho, F. Jelezko, E. Bielejec, H. Park, M. Lonar, and M. D. Lukin, *Science* **354**, 847–850 (2016).
16. O. Gazzano, and C. Becher, *arXiv preprint arXiv:1603.04529* (2016).
17. H. Clevenson, M. E. Trusheim, C. Teale, T. Schröder, D. Braje, and D. Englund, *Nature Physics* **11**, 393–397 (2015).
18. J. Burghoff, C. Grebing, S. Nolte, and A. Tunnermann, *Appl Phys Lett* **89**, 081108 (2006).
19. C. Hnatovsky, R. S. Taylor, E. Simova, V. R. Bhardwaj, D. M. Rayner, and P. B. Corkum, *Journal of Applied Physics* **98**, 013517 (2005).
20. Y.-f. Meng, C.-s. Yan, J. Lai, S. Krasnicki, H. Shu, T. Yu, Q. Liang, H.-k. Mao, and R. J. Hemley, *Proceedings of the National Academy of Sciences* **105**, 17620–17625 (2008).
21. A. Benayas, D. Jaque, B. McMillen, and K. P. Chen, *Journal of Applied Physics* **107**, 033522 (2010).
22. A. Ródenas, G. Torchia, G. Lifante, E. Cantelar, J. Lamela, F. Jaque, L. Roso, and D. Jaque, *Applied Physics B* **95**, 85–96 (2009).
23. R. Kalish, A. Reznik, S. Prawer, D. Saada, and J. Adler, *physica status solidi (a)* **174**, 83–99 (1999).
24. A. C. Ferrari, and J. Robertson, *Physical Review B* **61**, 14095–14107 (2000).
25. P. Olivero, F. Bosia, B. Fairchild, B. Gibson, A. Greentree, P. Spizzirri, and S. Prawer, *New Journal of Physics* **15**, 043027 (2013).

26. J. C. Lee, D. O. Bracher, S. Y. Cui, K. Ohno, C. A. McLellan, X. Y. Zhang, P. Andrich, B. Aleman, K. J. Russell, A. P. Magyar, I. Aharonovich, A. B. Jayich, D. Awschalom, and E. L. Hu, *Appl Phys Lett* **105**, 261101 (2014).
27. K. Ohno, F. J. Heremans, L. C. Bassett, B. A. Myers, D. M. Toyli, A. C. B. Jayich, C. J. Palmstrom, and D. D. Awschalom, *Appl Phys Lett* **101**, 082413 (2012).